Frontiers in Health Informatics www.healthinformaticsjournal.com
ISSN-Online: 2676-7104
2024; Vol 13: Issue 5 Open Access

Comparison of Photo Degradation Efficiency of Ce/Fe/TiO_2 Composite Catalyst Under UV and Visible Light Towards Evans Blue Dye

Loganathan A[1]., Kalaiyarasi C[2]., Dhilip P[3]., Mahalingam P[4], Murugesan B[5], Sivakumar P[6]

[1*]Department of Chemistry, Thiruvalluvar Govt. Arts College, Namakkal, TN, India – 637 401
[2,4,6]Department of Chemistry, Arignar Anna Govt. Arts College, Namakkal, TN, India – 637 002
[3]Department of Chemistry, Muthayammal College of Arts & Science, Rasipuram, TN, India - 637 408.
[5]Department of Chemistry, K.S.R College of Engineering, Tiruchengode, TN, India – 637215

***Correspondence Author:** Loganathan A
*Department of Chemistry, Thiruvalluvar Govt. Arts College, Namakkal, TN, India – 637 401

Cite this paper as: Loganathan (2024) A, Comparison of Photo Degradation Efficiency of Ce/Fe/TiO_2 Composite Catalyst Under UV and Visible Light Towards Evans Blue Dye. *Frontiers in Health Informatics*, 13 (5), 95-105

Abstract
This study investigates the synthesis and photocatalytic performance of a Ce/Fe/TiO_2 composite catalyst supported on nano carbon (NC), designated as Ce/Fe/TiO_2@NC, for the degradation of EB dye. The composite was characterized using X-ray diffraction (XRD) and scanning electron microscopy (SEM), which confirmed the successful incorporation of cerium, iron, and titanium dioxide in the NC matrix. XRD analysis revealed distinct peaks corresponding to the anatase phase of TiO_2, cerium oxide, and iron, indicating the formation of the composite. The photocatalytic activity of Ce/Fe/TiO_2@NC was evaluated under both UV and visible light irradiation, showing significant dye degradation, with 90.91% degradation under UV light at a dye concentration of 20 mg/L. The results suggest that Ce/Fe/TiO_2@NC is a highly efficient photocatalyst for organic pollutant degradation, offering potential applications in environmental remediation and wastewater treatment.

1.0 Introduction

Water pollution occurs when polluting substances such as chemicals, microorganisms or waste products contaminate water bodies. This pollution results in adverse effects on aquatic ecosystems and human health. Generally, sewage, industrial discharges, agricultural wastes and solid wastes cause pollution in rivers, lakes and oceans. This type of surface water pollution greatly affects drinking water supply and aquatic life [1]. Often runoff from landfills, poorly constructed waste disposal systems, or agricultural chemicals such as pesticides and fertilizers contaminates groundwater [2]. Oil spills, plastic waste and untreated sewage pollute seas and oceans. This type of pollution has devastating effects on marine biodiversity, including coral reefs and marine life. Chemical pollution occurs when toxic substances such as pesticides, heavy metals (mercury, lead) or industrial chemicals enter water systems. These pollutants can cause serious health problems including cancer, neurological damage and reproductive problems. Discharge of plastic debris, especially microplastics, into water bodies has become a major environmental problem. Plastics harm marine life, enter the food chain and affect the environment and human health [3-5].

Water treatment involves chemical, physical and biological processes. This purified water is used in various ways. Physical treatment removes solids from water using filters made of sand, peat or gravel. Various chemical treatment methods such as chlorination, ozonation, coagulation and flocculation, processes such as reverse osmosis remove dissolved salts, chemicals and other contaminants. Different types of biological treatment methods use specific bacteria or algae to break down organic pollutants and contaminants in wastewater, often in conjunction with other treatment methods [6].

In advanced purification methods, ultraviolet radiation uses ultraviolet light to disinfect water that kills bacteria and viruses without the use of chemicals. Photocatalysis is an advanced, sustainable treatment method that uses

light (usually ultraviolet) and a catalyst to accelerate chemical reactions that degrade pollutants in wastewater. This process uses the energy of light to generate highly reactive species such as hydroxyl radicals (•OH), which can break down organic and inorganic contaminants in water [7]. Catalysts used in photocatalysts such as TiO_2, ZnO, CeO2 etc are stable, non-toxic and reusable, making the method cost-effective in the long run. Photocatalysis can be used for both drinking water and industrial wastewater treatment, including the removal of heavy metals, dyes, and pharmaceutical residues [8].

Titanium dioxide and other common photocatalysts must activate primarily UV light. Since UV light makes up only a small fraction of sunlight, efforts are being made to develop catalysts that can operate under visible light. Researchers are exploring the use of doped photocatalysts (eg, doping TiO_2 with metals such as platinum or nitrogen) to improve performance under visible light [9].

Water pollution is a significant environmental problem, and its various forms require different treatment methods. Traditional methods such as filtration, chlorination, and biological treatment are commonly used, but as the problem nature of pollutants increases, advanced techniques such as photocatalysis are gaining attention. Photocatalysis, particularly the use of titanium dioxide as a catalyst, provides a promising method to effectively treat wastewater by breaking down organic pollutants under light [10]. Despite some challenges, current research is improving its efficiency and applicability, making it an important tool for modern wastewater treatment.

2.0 Materials and Methods

2.1 Preparation of Nano carbon (NC)

The waste diesel oil is burnt from the bottom using LPG as fuel mixed with air with the help of an indigenous CVD assembly. The waste oil will start to burn at its ignition temperature, then the fuel gas (LPG) was cut off and the air inlet is regulated in such a way that, the combustion temperature was controlled at 420 to 470°C. The soot formed during the combustion was collected using a dome shaped surface of chromium oxide layer of Stainless steel lid (316SS) which is kept over the combustion chamber. The excess flue gas was allowed to pass through the exhaust vents. Any ash formed during the combustion process was frequently removed through the discharge opening provided at the bottom of the reactor. The carbon deposited at the inner surface of stainless steel dome was carefully collected was washed with double distilled water and finally with alcohol.

2.2 Preparation of Ce/Fe/TiO_2@NC

About 17 ml of $(Ti(OBu)_4)$ was dissolved in 22 ml of ethanol with constant stirring and 1.5 ml of acetic acid was added drop-wise to suppress the hydrolysis. The above solution was stirred for 30 min using a magnetic stirrer to get the solution A. Solution B was prepared by adding 20 mL of 0.1M $Ce(NO)_3.6H_2O$ and 20 mL of 0.1M $Fe(NO)_3$. Prepared Solutions A and B were thoroughly mixed and the mixture was hydrolyzed at 25°C for about 30 min under agitation which yielded a transparent sol. Exactly 0.5g of NC is stirred well with using a magnetic stirrer for about half an hour. To this suspension, transparent sol containing Ce/Fe/TiO_2 was slowly added with constant stirring. After the addition of sol, the contents were stirred for 6 hrs and kept as such for further 24 h. After 24 h, the supernatant solution was decanted off and the contents were dried at 120°C until to get a solid mass. This was used in the subsequent adsorption and photocatalytic studies.

2.3 Characterization

X-ray diffraction (XRD) analysis was carried out for crystal phase identification of the TiO_2 samples using a Siemens D5000 diffractometer (Cu $K\alpha$ radiation). The phase composition was obtained from the XRD data using the software support program SIROQUANT. The morphology and particle size was determined under a transmission electron microscope (Phillips, CM200). The dispersion size was analysed by photon correlation spectroscopy on the Brookhaven 90+ instrument.

2.4 Photocatalytic studies

A stock solution of 1000 mg/L of adsorbate solution was prepared by dissolving 1.176 g of the respective dye in 1000 mL of distilled water. The stock solution was diluted to appropriate concentrations as and when required using distilled water. The structures of the dye selected for adsorption studies are shown in Figure 1 and some of its properties are given in Table 1. A Rayonet photochemical reactor (Ultraviolet Co., Model RPR-100) equipped with a UV lamp inside a chamber was used for the photocatalytic oxidation reactions.

The percentage and amount of dye removed through photocatalysis is calculated using the following relationships.

Percentage of dye removed = $\frac{Intial\ concentration(C_0) - Concentration\ at\ time\ t\ (C_t)}{Initial\ concentration\ (C_0)} x100$ (1)

Table 1 - Properties of Evans Blue Dye

Form	**Powder**
Molecular Formula	$C_{34}H_{24}N_6Na_4O_{14}S_4$
Colour	Blue
Odour	Nil
Colour index (CI Number)	23860
Maximum absorption wave length , λ max	611 nm
Classification	Anionic
Formula weight	960.82
Dye content	85%

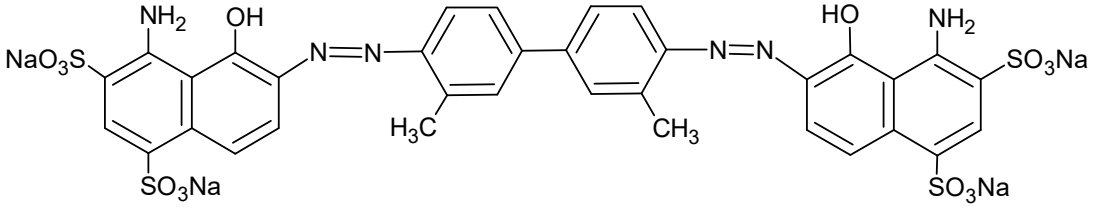

Figure 1 – Structure of Evans Blue dye

3.0 Results and Discussion

3.1 XRD Studies

The prepared samples were analyzed with XRD to ascertain the various crystallographic planes and evaluated the crystal forms of the composite catalyst (Figure 2). The XRD pattern of NC has a broad peak at 25° which is generated due to the reflections of (002) graphitic plane. This is a typical pattern of amorphous structure with a d_{002} of 0.036 nm based on Bragg's equation (JCPDS 41-1487), which gives a quantitative measurement for the graphitic network [11]. The Peaks for Anatase form of TiO_2 is observed at 25.3°, 48.0°, 53.9°. The peak at 54.57° for the (105) plane of anatase evidence the presence of doped Titania on the NC surface [12]. The Peaks substantiate the presence of Fe is observed at 65° and the Ce doping (111), (200) and (220) planes is also confirmed from the XRD peaks available at 28.6° and 33.2° [13].

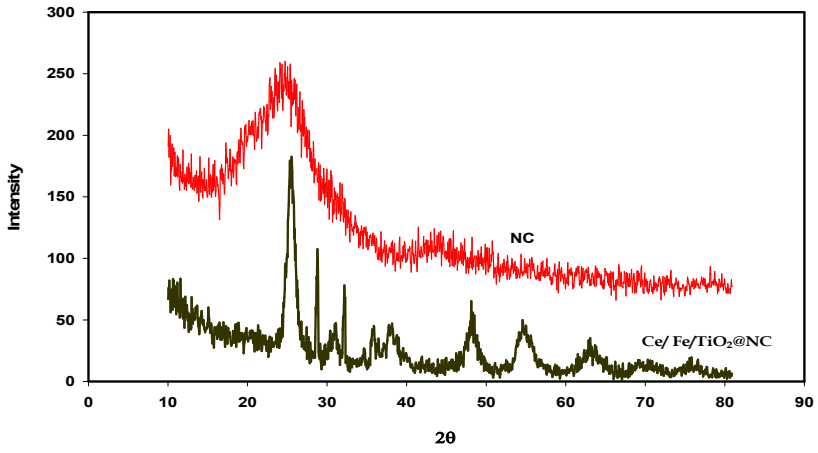

Fig. 2 – XRD Patterns of NC and Ce/Fe/TiO_2@NC

3.2 SEM Studies

The scanning electron microscopic images of NC and Ce/Fe/TiO_2@NC are shown in Figure 3. As observed from the SEM images of the pure carbon samples, the clusters of carbon nano spheres of sizes ranging between

50 and 80 nm are present. When the carbon is co-doped with Ce/Fe/TiO_2, the composite grains are uniformly distributed over the surface of NC [14].

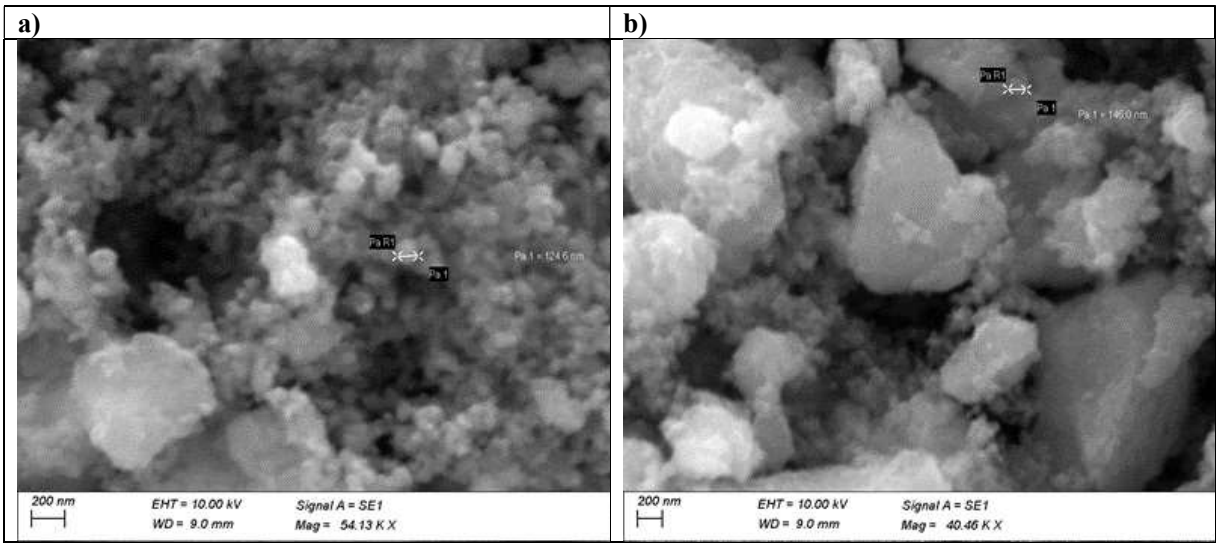

Fig. 3 – SEM Images of a) NC and b) Ce/Fe/TiO_2@NC

3.3 Dye Degradation Studies of Ce/Fe/TiO_2@NC Catalyst

The photocatalytic activity of Ce/Fe/TiO_2@NC is dependent on the size, morphology and crystal structure [15]. Semiconductor TiO_2 is proved as an efficient photo catalyst under solar irradiation. Carbon doped TiO_2 is found to have excellent photocatalytic character under solar irradiation [16]. Though the mechanism of enhancement of photocatalytic activity of TiO_2 by carbon doping is not clear, many researchers are working towards the development of carbon doped TiO_2 photo catalyst. The photocatalytic decomposition of EB dye is demonstrated in the subsequent section.

3.4 Effect of initial dye concentration

The role of the prepared Ce/Fe/TiO_2@NC composite for the degradation of EB was also investigated by varying the initial dye concentration from 20 to 60 mg/L and was presented in figure 4 and 5. The photo degradation of EB was 90.91 % under UV and 81.82 % under visible radiation at an initial EB concentration of 20 mg/l. At 60 mg/L of initial dye concentration the degradation of EB was changed into 95.12 % under UV irradiation, and 8.807 % under visible irradiation. Though the percentage degradation of EB was slightly low under visible irradiation when compared to UV irradiation, good amount of dye was degraded under visible irradiation. At higher concentrations, the effective penetration of light was prevented and the number of photons falling on the catalyst surface decreased, which ultimately reduced the performance of catalysts [17&18].

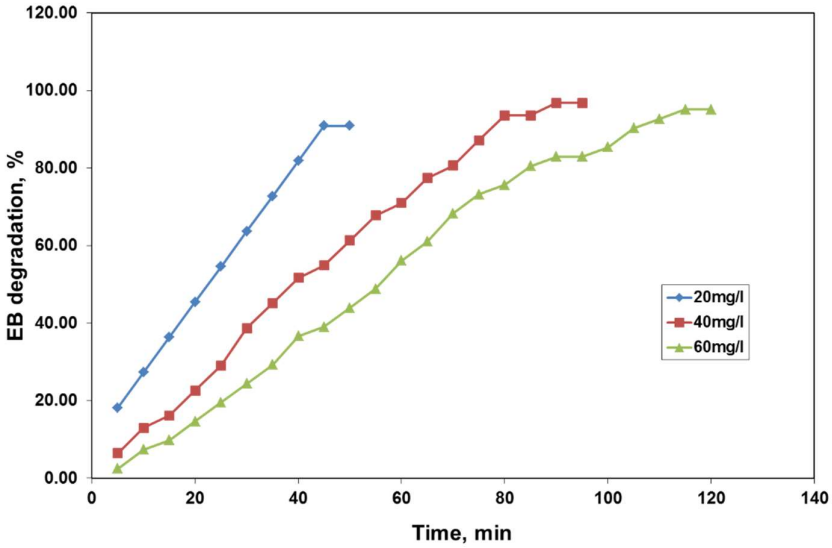

Fig. 4 – Effect of initial dye concentration on the degradation of EB – UV light

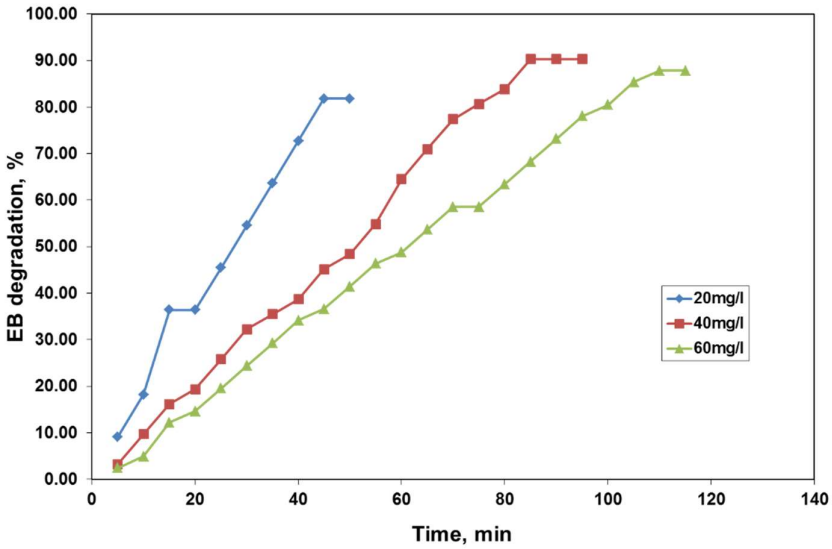

Fig. 5 – Effect of initial dye concentration on the degradation of EB – Visible light

3.5 Effect of pH

The effect of solution pH for the photocatalytic degradation of EB was shown in figure 6 for pH range of 1.0 to 11. Under UV and Visible irradiation, the decomposition percentage of EB decreased with an increase of pH from 1 to 11. The reason for the low degradation at higher pH was mainly because of the fundamental mechanisms involved in the TiO_2 process. At low pH range, oxidation by the positive holes present of the surface of Ce/Fe/TiO_2@NC predominant mechanism. At the high pH range, the hydroxyl radical played a dominant role in the oxidative decomposition of EB [18&19]. Similar mechanisms had been proposed by many researchers earlier for the photo oxidation of other organic pollutants. Tunesi and Anderson proposed similar pathways under acidic and basic conditions for the photocatalytic oxidation of salicylic acid using TiO_2 [20].

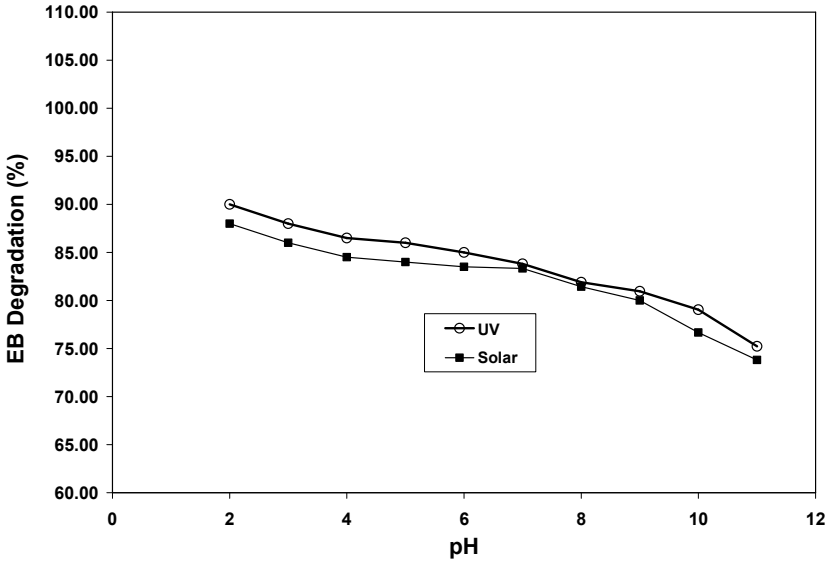

Figure 6 – Effect of pH on the degradation of EB

3.6Effect of catalyst load

Optimizing the catalyst load for any industrial catalyzed process is an essential one. The optimal concentration of catalyst depends on many factors like working conditions, surface area of the catalyst, the wavelength of the incident radiation etc. The optimum amount of catalyst required for the effective oxidative degradation of EB dye by Ce/Fe/TiO_2@NC was carried out by studying the decomposition at various catalyst loads. The experiment was carried out with a catalyst loading of 100 to 500mg for 100 ml of dye solution of specified concentration at the natural pH of the dye solution.

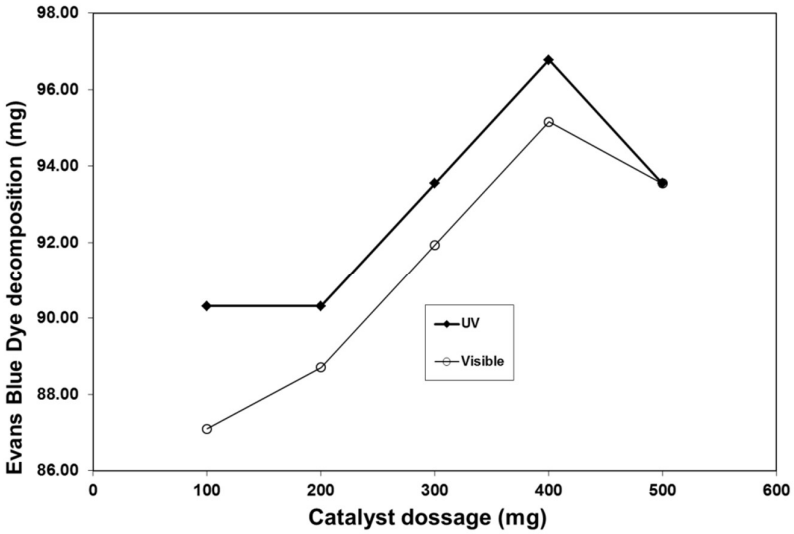

Figure 7 – Effect of catalyst dosage on the degradation of EB

For the optimization of catalyst loading, the contents were left for 5 hours and the final concentration of the dye solution was analyzed spectro-photometrically after removing the catalyst by centrifugation. The catalyst dosage on the degradation of EB under UV and Visible was shown in figure 7. The percentage of EB degradation increased from 96.77 and 95.16 % while increasing the catalyst load from 100 to 500mg and further increase in the catalyst load decreased the photo degradation of EB dye. The decrease in photo degradation of EB when the catalyst load went above 400mg due to the fact that the high concentration of catalyst prevented

the effective photo-absorption and thereby reduced the photo degradation [21-23]. Therefore, 400mg catalyst load was fixed as the optimum level for further photocatalytic degradation of EB.

3.7 Kinetic Model to predict the rate constant for the photodegradation

The rates of photocatalytic degradation of organic molecules are independent of the concentration of the hydroxide ion. Therefore the experimental data were analyzed using the following pseudo-first order kinetic expression.

$$\ln C_t = -k_1 t + \ln C_0$$

where C_0 is the initial concentration of EB dye (mg/L), C_t is concentration of EB at time t (mg/L) and k_1 is the pseudo-first order rate constant (min^{-1}). The pseudo-first order rate constant was determined from the slope of the plot $\ln C_t$ versus t as shown in figure 8 and 9.

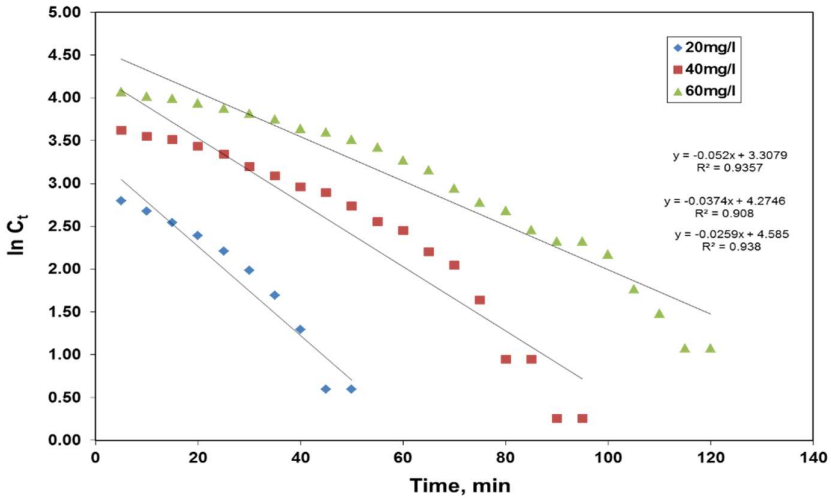

Figure 8 – Pseudo-first order plot of EB degradation under UV irradiation

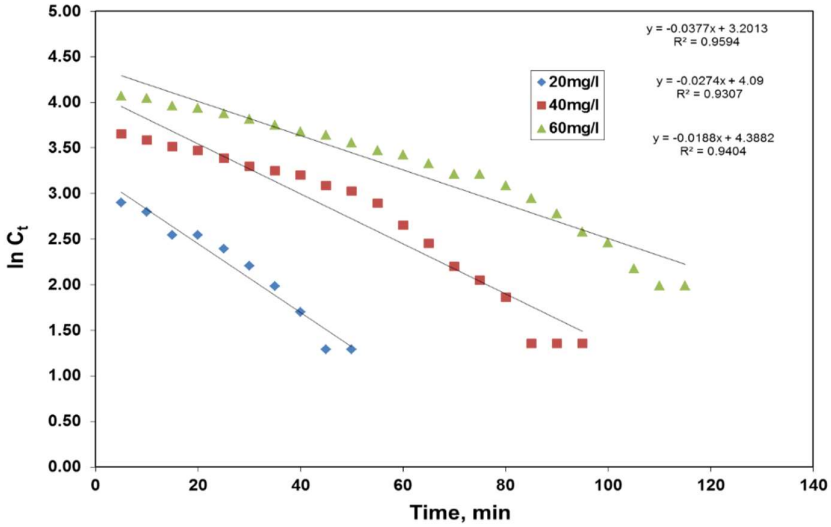

Figure 9 – Pseudo-first order plot of EB degradation under visible irradiation

The results of kinetic analysis indicated that the pseudo-first order rate constant decreased from 0.11976 to 0.05758 under UV irradiation; and it also decreased from 0.08521 to 0.04145 under visible irradiation while increasing the initial dye concentration from 20 to 60 mg/L. The correlation coefficient of pseudo-first order kinetics were found to be $0.938 < r^2 < 0.902$ under UV irradiation and $0.959 < r^2 < 0.940$ under visible irradiation. As the initial dye concentration increased, the effective light penetration was prevented due to scattering of photons by the dye molecules, which resulted in reduction of the first order rate constant [24]. Both under the

UV and visible irradiation, the photocatalytic decomposition of EB by Ce/Fe/TiO_2@NC composite followed the pseudo-first order kinetics with good correlation coefficient.

The pseudo-second order kinetic model can be expressed as

$$1/C_t = k_2 t + 1/C_0$$

where k_2 is the pseudo-second order rate constant and it was determined from the slope of the plot $1/C_t$ vs. t as shown in figure 10 and 11. The results of the kinetic studies were presented in table 2.

Table 2 – Results of the photodegradation kinetics of EB by Ce/Fe/TiO_2@NC

UV irradiation				
Initial dye concentration, mg/L	**k_1 Sec^{-1}**	**r^2**	**$k_2 \times 10^{-4}$ (g/mg/min)**	**r^2**
20	0.11976	0.935	13.297	0.764
40	0.08521	0.908	2.3529	0.609
60	0.05758	0.938	0.7547	0.653
Visible Irradiation				
20	0.08521	0.959	50.000	0.856
40	0.06218	0.930	1.1429	0.755
60	0.04145	0.940	1.2500	0.757

On analyzing the kinetics of photocatalytic decomposition of EB by Ce/Fe/TiO_2@NC composite catalyst, it was observed that the pseudo-second order rate constant decreases from 13.294 x 10^{-4} to 0.7547 x 10^{-4} (g/mg/min) under UV irradiation and 50.00 x 10^{-4} to 1.250 x 10^{-4} (g/mg/min) under visible light irradiation while increasing the initial dye concentration from 20 to 60 mg/L.

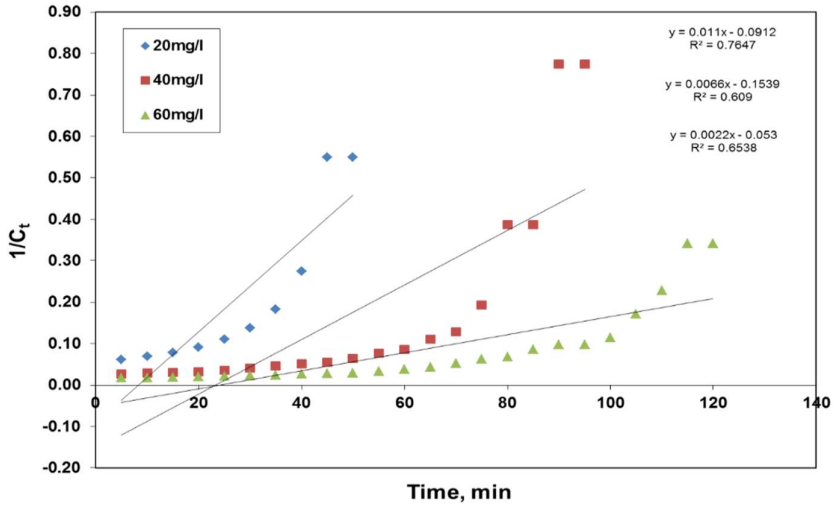

Figure 10 – Pseudo-second order plot of EB degradation under UV irradiation

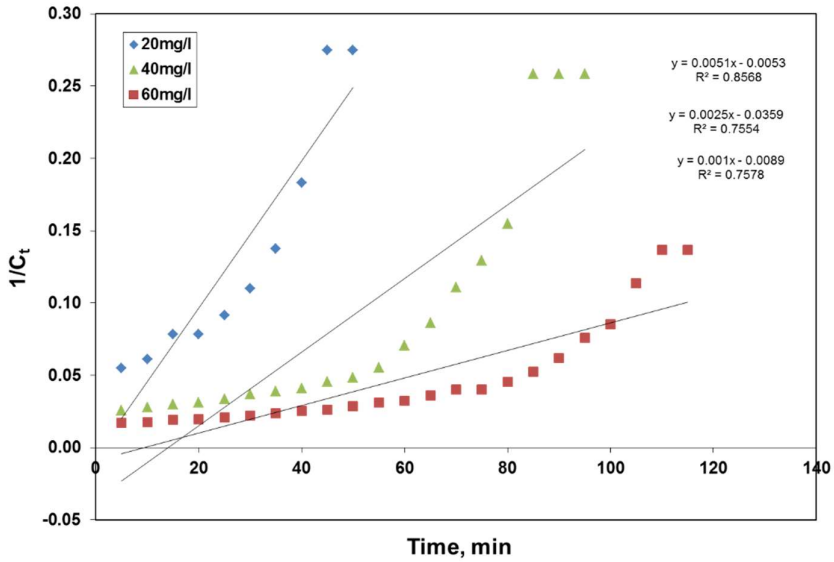

Figure 11 – Pseudo-second order plot of EB degradation under visible irradiation

The regression coefficient (r^2) for the pseudo-second order kinetic model is lower than the pseudo-first order kinetic model under UV and visible light irradiation. It was clear that the pseudo-first order kinetic model is more appropriate to explain the photocatalysis than pseudo-second order kinetic model [25&26].

4.0 Conclusion

The study effectively demonstrates the synthesis and characterization of the Ce/Fe/TiO_2@NC composite catalyst and evaluates its photocatalytic performance for dye degradation. X-ray diffraction (XRD) analysis confirmed the successful incorporation of cerium (Ce), iron (Fe), and titanium dioxide (TiO_2) into the carbon nanotube (NC) structure, with distinct peaks corresponding to the anatase form of TiO_2, cerium oxide (CeO_2), and iron. The photocatalytic activity of Ce/Fe/TiO_2@NC was tested for the degradation of EB dye under varying conditions such as dye concentration, pH, and catalyst load. The results indicated that the composite catalyst showed significant photocatalytic activity under UV light, with degradation rates as high as 90.91% at low dye concentrations. The study also highlighted the influence of solution pH and catalyst load on photocatalytic performance. Kinetic analysis using pseudo-first-order and pseudo-second-order models revealed that the photocatalytic degradation followed pseudo-first-order kinetics, with good correlation coefficients, making it a reliable method for predicting the degradation rate. The composite's high efficiency, coupled with its stability and reproducibility, suggests its potential for practical applications in wastewater treatment and environmental remediation.

References

1. Chowdhary, P., Bharagava, R. N., Mishra, S. & Khan, N. Role of Industries in Water Scarcity and Its Adverse Effects on Environment and Human Health. In Environmental Concerns and Sustainable Development (2020) 235–256.
2. Parris, K. Impact of agriculture on water pollution in OECD countries: Recent trends and future prospects. International Journal of Water Resources Development, 27 (2011) 33–52.
3. Beaumont, N. J. et al. Global ecological, social and economic impacts of marine plastic. Mar Pollut Bull, 142 (2019) 189–195.
4. Kamran, S. et al. Heavy Metals Contamination and what are the Impacts on Living Organisms. Greener Journal of Environmental Management and Public Safety, 2 (2013) 172–179.
5. Rout, C. & Sharma, A. Oil Spill in Marine Environment: Fate and Effects. 2nd International Conference on Evolution in Science & Technology & Eyne on Educational Methodologies. (2013).
6. Crini, G. & Lichtfouse, E. Advantages and disadvantages of techniques used for wastewater treatment. Environmental Chemistry Letters, 17 (2019) 145-155.

7. Wang, X. Q., Han, S. F., Zhang, Q. W., Zhang, N. & Zhao, D. D. Photocatalytic oxidation degradation mechanism study of methylene blue dye waste water with GR/iTO$_2$. In MATEC Web of Conferences. 238 (2018).
8. Fang, S. et al. Facile synthesis of CeO_2 hollow structures with controllable morphology by template-engaged etching of Cu_2O and their visible light photocatalytic performance. Applied Catalysis B. 179 (2015)458–467.
9. Huang, F., Yan, A. & Zhao, H. Influences of Doping on Photocatalytic Properties of TiO_2 Photocatalyst. In Semiconductor Photocatalysis - Materials, Mechanisms and Applications (2016).
10. Heng Z, Hao W, Caiyan Y, Lijuan H, Hui L, Heng Z, Song Y, Tianyi M. Photocatalytic degradation by TiO_2-conjugated/coordination polymer heterojunction: Preparation, mechanisms, and prospects. Applied Catalyst B: Environmental and Energy, 344 (2024), 123605.
11. Tran V K, Pham T, Le N, Le V, Tran D, Vuong V & Mai T. Effect of hydrothermal time on the structure and property of graphene oxide membrane. Journal of Ceramic Processing Research. 22 (2021) 425-435.
12. Velmurugan, R., Krishnakumar, B., Kumar, R. & Swaminathan, M. Solar active nano-TiO $_2$ for mineralization of Reactive Red 120 and Trypan Blue. 1st Nano Update. Arabian Journal of Chemistry. 5 (2012) 447–452.
13. Wang, F., Li, D. & Mao, J. Control of exposed crystal planes of CeO_2 enhances electrocatalytic nitrate reduction. Microstructures. 4 (2024).
14. Bojarski, S. A., Stuer, M., Zhao, Z., Bowen, P. & Rohrer, G. S. Influence of y and la additions on grain growth and the grain-boundary character distribution of alumina. Journal of the American Ceramic Society. 97 (2014) 622–630.
15. Tuc Altaf, C Tuc Altaf C, Olcayto Colak T, Mihai Rostas A, Popa A, Toloman D, Suciu M, Demirci Sankir N and Meh. Impact on the Photocatalytic Dye Degradation of Morphology and Annealing-Induced Defects in Zinc Oxide Nanostructures. ACS Omega. 8 (2023) 14952–14964.
16. Kumar R, Choudhary R, Kolay S, Pandey P , Singh K and Bhargava P. Carbon coated titanium dioxide (CC-TiO_2) as an efficient material for photocatalytic degradation. Energy Advances. (2022) 926–934.
17. Montazerghaem, L., Keramatifarhodbonab, M. & Naeimi, A. Photocatalytic degradation of acid blue 74 by Co: WO_3 nanoparticles: Kinetics and response surface methodology studies. Heliyon. 10 (2024).
18. Siddique, M., Khan, R., Farooq, R. & Khan, A. F. Improved Photocatalytic Activity of TiO_2 Coupling Ultrasound for Reactive Blue 19 Degradation. Journal of the Chemical Society of Pakistan. 36 (2-014).
19. El-Naggar, M. A., Maghawry. A, Alturki. A, Nosier. A, Hussein. M & Abdel-Aziz. M. TiO_2-catalyzed photodegradation of methylene blue in a helical FEP tubing reactor: modeling and optimization using response surface methodology. Applied Water Science. 14, (2024).
20. Tunesi. S & Anderson. M. Influence of chemisorption on the photodecomposition of salicylic acid and related compounds using suspended titania ceramic membranes. The Journal of Physical Chemistry. 95 (1991).
21. Toor, A. T., Verma, A., Jotshi, C. K., Bajpai, P. K. & Singh, V. Photocatalytic degradation of Direct Yellow 12 dye using UV/TiO_2 in a shallow pond slurry reactor. Dyes and Pigments. 68 (2006) 53–60.
22. Jithendra Kumara K. S, Krishnamurthy. G, Walmik. P, Naik. S, Priya Rani S. R & Naik. N. Synthesis of reduced graphene oxide decorated with Sn/Na doped TiO_2 nanocomposite: a photocatalyst for Evans blue dye degradation. Emergent Materials. 4 (2021) 457-468.
23. Zhu. H, Jiang. R, Xiao. L, Chang. Y, Guan. Y, Li. X & Zeng. G. Photocatalytic decolorization and degradation of Congo Red on innovative crosslinked chitosan/nano-CdS composite catalyst under visible light irradiation. J Hazard Mater. 169 (2009) 933–940.
24. Jadaa, W., Prakash, A. & Ray, A. K. Photocatalytic degradation of diazo dye over suspended and immobilized TiO_2 catalyst in swirl flow reactor: Kinetic modeling. Processes. 9 (2021).
25. Al-Harby, N. F., Albahly, E. F. & Mohamed, N. A. Kinetics, isotherm and thermodynamic studies for efficient adsorption of congo red dye from aqueous solution onto novel cyanoguanidine-modified chitosan adsorbent. Polymers (Basel). 13 (2021).
26. Aisien, F., Amenaghawon, A. N., Aisien, F. A., Amenaghawon, N. A. & Urhobotie, O. I. Potential Application of a Locally Sourced Photocatalyst for the Photocatalytic Decolourisation of Methyl Orange in Aqueous Solution. Journal of Engineering Science and Technology. 10 (2015).